Hydrothermal Synthesis and Characterization of Nanorods of Various Titanates and Titanium Dioxide

Yury V. Kolen'ko,*,†,‡ Kirill A. Kovnir,†,§ Anton I. Gavrilov,† Alexei V. Garshev,† Johannes Frantti,‡,∥ Oleg I. Lebedev,⊥,# Bulat R. Churagulov,○ Gustaaf Van Tendeloo,⊥ and Masahiro Yoshimura‡

Department of Materials Science, Moscow State University, Moscow 119992, Russia, Materials and Structures Laboratory, Tokyo Institute of Technology, 4259 Nagatsuta, Midori-ku, Yokohama 226-8503, Japan, EMAT, University of Antwerp, Groenenborgerlaan 171, Antwerpen B-2020, Belgium, and Department of Chemistry, Moscow State University, Moscow 119992, Russia

Received: October 5, 2005; In Final Form: January 10, 2006

The formation process of titania based nanorods during hydrothermal synthesis starting from an amorphous $TiO_2 \cdot nH_2O$ gel has been investigated. Sodium tri-titanate ($Na_2Ti_3O_7$) particles with a rodlike morphology were prepared by a simple hydrothermal process in the presence of a concentrated NaOH aqueous solution. The ion exchange reaction of the synthesized $Na_2Ti_3O_7$ nanorods with HCl under ultrasonic treatment promotes a complete sodium substitution and the formation of $H_2Ti_3O_7$ nanorods. Low-temperature annealing of the as-produced nanorods of $Na_2Ti_3O_7$ and $H_2Ti_3O_7$ leads to a loss of the layered crystal structure and the formation of nanorods of condensed framework phases—sodium hexa-titanate ($Na_2Ti_6O_{13}$) and metastable TiO_2-B phases, respectively. These transformations proceed without a significant change in particle morphology. The nanostructures were investigated by scanning electron microscopy (SEM), powder X-ray diffraction (XRD), the Brunauer−Emmett−Teller (BET) method, thermogravimetric analysis (TGA), and Raman spectroscopy. The structural defects of the synthesized nanorods were investigated by high-resolution electron microscopy. The presence of planar defects can be attributed to the exfoliation of the zigzag ribbon layers into two-dimensional titanates as well as to the condensation of the layers of TiO_6 octahedra into three-dimensional frameworks.

Introduction

In the past decade, design and fabrication of nanostructures based on metal oxides has attracted much attention because of their peculiar electronic and optical properties and their potential applications in industry and technology.[1] One of the most intensively studied oxides is titania. Over the past few years, a large number of experimental approaches have been successfully used as routes to synthesize nanorods or nanowires based on titania, such as combining sol−gel processing with electrophoretic deposition,[2] the spin-on process,[3] the sol−gel template method,[4] metalorganic chemical vapor deposition,[5] anodic oxidative hydrolysis,[6] sonochemical synthesis,[7] the inverse microemulsion method,[8] and efficient molten salt-assisted and pyrolysis routes.[9] Recently, hydrothermal synthesis[10] of the rodlike nanostructures based on titania has attracted much attention. The advantage of this technique is that nanorods can be obtained in relatively large amounts.

Hydrothermal treatment of different TiO_2 precursors in a highly alkaline medium is a powerful way to prepare nanotubes and nanowires based on titania. For example, nanowires of $K_2Ti_6O_{13}$ have been successfully prepared by the hydrothermal route using KOH.[11] Nanorods and nanotubes might also be prepared using NaOH, but the information about the structure of the synthesized nanostructures is still unclear despite intensive investigations. It was first believed that, in the case of hydrothermal synthesis with NaOH, the products are nanotubes and nanorods of anatase.[12] Later, it was shown that nanotubes of $H_2Ti_3O_7$ are formed that contain no sodium and NaOH only acts as a catalyst.[13] It was also concluded that washing with distilled water does not lead to removal of the sodium from the synthesized particles, since washing in water, ethanol, and acetone gives the same results.[13b] In contradiction with previous investigations, Sun et al.[14] report that as-synthesized nanotubes are titanates and can be described as $Na_xH_{2-x}Ti_3O_7$. Thermal treatment of these materials leads to the formation of different titanates with the general formula $Na_2Ti_nO_{2n+1}$. Recently, it was also mentioned that as-synthesized nanotubes or nanorods have an even more complex structure, namely, $Na_xH_{2-x}Ti_nO_{2n+1} \cdot yH_2O$.[15] Treatment of these nanoparticles with a HCl solution produced nanotubes and nanorods of $H_2Ti_3O_7$. It was also demonstrated that the thermal behaviors of these two types of nanostructures are different. While nanotubes upon heating in air transform to anatase and lose their morphology, the nanorods

* Corresponding author. Mailing address: Dr. Yury V. Kolen'ko, R3-20, Center for Materials Design, Materials and Structures Laboratory, Tokyo Institute of Technology, 4259 Nagatsuta, Midori-ku, Yokohama 226-8503, Japan. Phone: +81-(0)45-924-5368. Fax: +81-(0)45-924-5358. E-mail: kolenko@msl.titech.ac.jp.

† Department of Materials Science, Moscow State University.

‡ Tokyo Institute of Technology.

§ Present address: Max-Plank-Institute for Chemical Physics of Solids, Dresden 01187, Germany.

∥ Present address: Laboratory of Physics, Helsinki University of Technology, P. O. Box 1100, FIN-02015 HUT, Finland.

⊥ University of Antwerp.

On leave from the Institute of Crystallography RAS, Moscow 117333, Russia.

○ Department of Chemistry, Moscow State University.

10.1021/jp055687u CCC: $33.50
Published on Web 02/14/2006

TABLE 1: Phase Composition and Size Distribution of Nanorods Synthesized by Hydrothermal Treatment of $TiO_2 \cdot nH_2O$ in 10 mol/L NaOH Solution

reference	conditions (T, t) of hydrothermal synthesis or *annealing*	further processing or atmosphere	nanorod size distribution,[a] SEM/TEM (±10%) W/nm	L/μm	phase composition
NR-1	200 °C, 20 h	no	~70−1400	~0.4−15	$Na_2Ti_nO_{2n+1}$ (n = 3, 4, 9)
NR-2	200 °C, 20 h	8 min of US[b] treatment in 0.1 mol/L HCl two times	~80−1300	~1−12	$H_2Ti_3O_7$
		Annealed Samples			
NR-1-HYD	*500 °C, 10 h*	hydrogen flow	~90−1500	~0.2−22	$Na_2Ti_6O_{13}$
NR-2-AIR	*500 °C, 10 h*	air	~80−600	~0.1−8	TiO_2-B

[a] W, width; L, length. [b] US, ultrasonic.

convert to another modification of titania, the metastable TiO_2-B phase, and retain their cylindrical-like morphology.

The aim of this work is to examine the formation of nanorods by the reaction of an amorphous $TiO_2 \cdot nH_2O$ gel and a concentrated NaOH solution under hydrothermal conditions. We report the synthesis of nanorods of sodium tri-titanate ($Na_2Ti_3O_7$) and hydrogen titanate ($H_2Ti_3O_7$) phases based on a simple hydrothermal route. The crystal structure of the synthesized nanorods can be appreciably modified without significant changes to the particle morphology. We report the transformation of these layered compounds into three-dimensional frameworks—sodium hexa-titanate ($Na_2Ti_6O_{13}$) and titanium dioxide (TiO_2-B) phases.

Experiment

Materials. Analytical grade NH_3 25% (aq.), HCl, distilled water, and $TiCl_4$ (>99%, "Merck") were used for the preparation of raw amorphous titania material—$TiO_2 \cdot nH_2O$ gel. It was made according to the following procedure: Titanium tetrachloride was added dropwise to a calculated amount of concentrated HCl (molar ratio $HCl/TiCl_4 = 2.1:1$) to form H_2TiCl_6. Then, the excess of ammonia solution (100 cm^3) was added to the H_2TiCl_6 solution (25 cm^3 of H_2TiCl_6 and 75 cm^3 of distilled water) under vigorous stirring. As a result of hydrolysis (pH 11.0), a white amorphous $TiO_2 \cdot nH_2O$ precipitate was obtained. The precipitate was filtered on a glass filter and washed with distilled water until the absence of residual Cl^- ions (tested by reaction with a $AgNO_3$ solution).

Hydrothermal Synthesis of Nanostructures. The synthesis of titania based nanostructures has been performed by the hydrothermal method using a chemical process similar to that described by Kasuga et al.[12] Amorphous $TiO_2 \cdot nH_2O$ gel (~2 g) was mixed with a NaOH aqueous solution (concentration of 10 mol/L) and placed in a poly(tetrafluoroethylene) lined autoclave (volume 55 cm^3, degree of filling 80%). Hydrothermal syntheses were performed at 110, 160, and 200 °C for 20 h. The products of the hydrothermal syntheses were isolated by centrifugation and then washed several times with distilled water.

Further Processing. The obtained powders were dispersed by ultrasonication (UZG-100 Ultrasonic Generator, Impul's Co.) in 75 cm^3 of 0.1 mol/L HCl aqueous solution for 8 min two times. The thermal treatment of the synthesized samples was carried out at 500 °C in an atmosphere of air or in a hydrogen flow (20 cm^3/min). The treatment included a 6 h heating to the final temperature and a 10 h isothermal annealing.

Throughout this work, a set of acronyms is used: **NR-1**, **NR-2**, **NR-1-HYD**, and **NR-2-AIR**. The first two letters (NR) stand for "nanorod", the number represents the sample number, and the last letters indicate the atmosphere of the thermal treatment at 500 °C for 10 h.

SCHEME 1

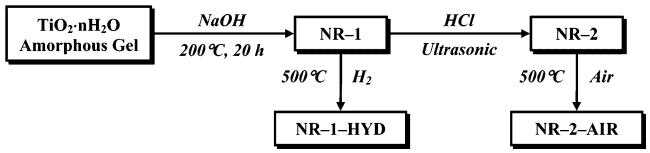

Characterization. After filtration and drying, the products were characterized by powder X-ray diffraction (XRD) using a Huber G670 Image Plate Camera (CuKα1 radiation, λ = 1.540598 Å). The morphology was studied by scanning electron microscopy (SEM) using a Leo Supra 50 VP microscope operating at 5 kV with an INCA Energy + spectrometer for energy-dispersive X-ray (EDX) spectroscopy operating at 20 kV. Transmission electron microscopy (TEM), electron diffraction (ED), and high-resolution electron microscopy (HREM) investigations confirm the formation of different crystal structure types and also reveal the defect structure. TEM and HREM were performed using a JEOL 4000 EX microscope operating at 400 kV. The samples for transmission electron microscopy were crushed, dispersed in methanol, and deposited on a holey carbon grid. Image simulations were obtained using the MacTempas software. The room temperature Raman scattering measurements were carried out on a Jobin Yvon T64000 spectrometer with visible laser light (wavelength 514.532 nm) as the excitation light. The slits were adjusted so that the resolution was 1 cm^{-1}. The scattered light was collected in the backscattering geometry using a liquid nitrogen cooled CCD detector. All measurements were carried out under the microscope (the laser spot diameter was estimated to be between 1 and 2 μm). Prior to each measurement, the spectrometer was calibrated using a mercury lamp. Thermogravimetric analysis (TGA) was performed using a Perkin-Elmer PYRIS Diamond TG-DTA thermoanalyzer, in air, at a heating rate of 10 °C/min. The specific surface area was measured by the multipoint Brunauer−Emmett−Teller (BET) method using N_2 as adsorbed gas on a Coulter SA 3100 instrument.

Results

Synthesis. Rodlike nanostructures were prepared by hydrothermal treatment of an amorphous $TiO_2 \cdot nH_2O$ gel with a 10 mol/L NaOH solution. The synthesis conditions, phase composition, and size distribution of the hydrothermal derived nanorods are given in Table 1, and in Scheme 1 all of the synthetic procedures are summarized. Several additional syntheses were performed at lower temperatures (110 and 160 °C), as described in the experimental part.

SEM, EDX, and BET. Figure 1A shows a typical SEM image of the **NR-1** sample. The nanorods are mostly continuous and arranged roughly parallel to their axes. They exhibit a nonuniform size distribution: a width of about 70−1400 nm and a length in the range from 0.4 to 15.0 μm. A following

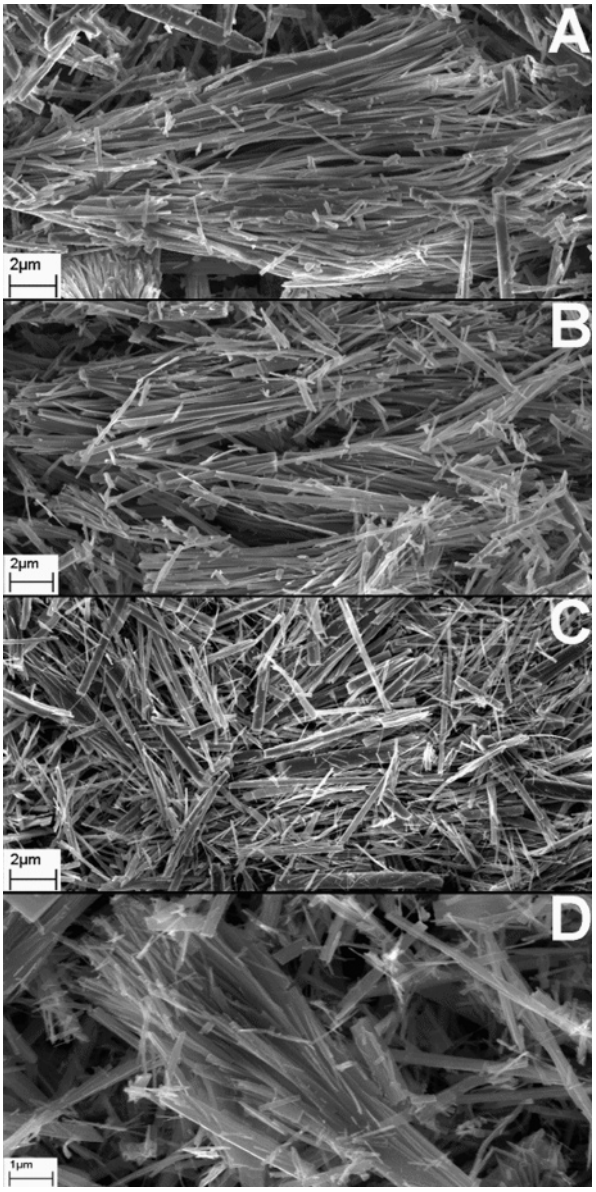

Figure 1. SEM images of the synthesized nanorods: (A) **NR-1**; (B) **NR-1-HYD**; (C) **NR-2**; (D) **NR-2-AIR**.

treatment of the **NR-1** sample by ultrasonic dispersion of the product in 0.1 M HCl leads to a similar morphology. SEM observations (Figure 1C) reveal a large quantity of rodlike nanostructures in the **NR-2** sample with typical widths in the range of several tens of nanometers to several hundred nanometers and with typical lengths in the range of several micrometers to several tens of micrometers (see Table 1). The nanorods size distribution is also similar to that of sample **NR-1**. The specific surface area of sample **NR-2** is relatively low (18 m^2/g) which is typical for nanopowders with a high crystallinity. The EDX analysis of **NR-1** confirms the presence of sodium in the sample. The average contents of titanium and sodium are ~22.7 and ~12.7 atom % (ratio Ti/Na ~ 1.8). At the same time, the EDX analysis reveals the presence of only titanium and oxygen in sample **NR-2**.

Annealing of sample **NR-1** in a hydrogen flow and sample **NR-2** in air at 500 °C (see Scheme 1, samples **NR-1-HYD** and **NR-2-AIR**, respectively) does not lead to significant changes of the microstructure (Figure 1B and D). No morphology changes are observed, while a decrease of the average size and a narrowing of the size distribution of the nanorods occur during transformation of sample **NR-2** to sample **NR-2-AIR** (see Table 1).

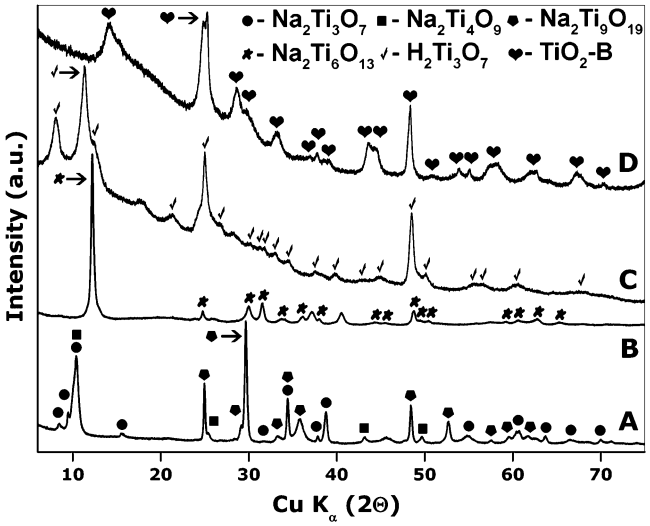

Figure 2. Powder X-ray diffraction patterns of the titania based nanorods: (A) **NR-1**; (B) **NR-1-HYD**; (C) **NR-2**; (D) **NR-2-AIR**.

SEM measurements show that a hydrothermal treatment of the amorphous $TiO_2 \cdot nH_2O$ gel at 110 and 160 °C for 20 h followed by an ultrasonic dispersion in 0.1 M HCl does not result in the formation of nanostructures. The samples are highly amorphous. It should be noted that these samples possess a high specific surface area (320 and 260 m^2/g, respectively) which is typical for substances in an amorphous state.

Powder X-ray Diffraction. All samples have typical XRD patterns for nanopowders with high background and broad peaks.

***NR-1** Sample.* The powder XRD pattern of the sample reveals the overall crystalline structure of the nanorods (Figure 2A). According to the phase analysis, sample **NR-1** is a mixture of three sodium titanates ($Na_2Ti_nO_{2n+1}$, $n = 3, 4, 9$) (JCPDS nos. 31-1329, 33-1294, and 33-1293).

***NR-2** Sample.* The powder XRD pattern of the sample is presented in Figure 2C. Most of the relatively sharp peaks belong to the layered hydrogen titanate ($H_2Ti_3O_7$; monoclinic, $a = 1.603$ nm, $b = 0.375$ nm, $c = 0.919$ nm, $\beta = 101.45°$).[16] However, there are some inconsistencies between the intensity of the diffraction peaks reported in the literature and the observed ones;[16] this is caused by the finite size of the particles, possible texturing of needlelike particles, and various structural defects (vide infra).

Samples synthesized by hydrothermal treatment at 110 and 160 °C for 20 h followed by an ultrasonic dispersion in 0.1 M HCl are dominantly amorphous; however, powder XRD patterns exhibit some weak and extremely broad peaks corresponding to a hydrogen titanate ($H_2Ti_3O_7$).

***NR-1-HYD** Sample.* Phase analysis did not reveal the exact phase composition of the sample (Figure 2B). However, there are three compounds in the H/Na/Ti/O system that possess an XRD pattern closely related to the observed one: mixed-valence sodium titanate ($Na_xTi_2O_4$),[17] sodium hexa-titanate ($Na_2Ti_6O_{13}$),[18] and sodium hepta-titanate ($Na_2Ti_7O_{15}$).[19] The first compound is extremely air and moisture sensitive;[17] since we observed the same XRD pattern after 3 months of storing sample **NR-1-HYD** in air, $Na_xTi_2O_4$ can be excluded. Hexa-titanate and hepta-titanate have similar powder XRD patterns, and the quality of our X-ray data does not allow distinguishment among them. Moreover, a significant shift of several diffraction peaks is reported in the case of nanorods of sodium hexa-titanate

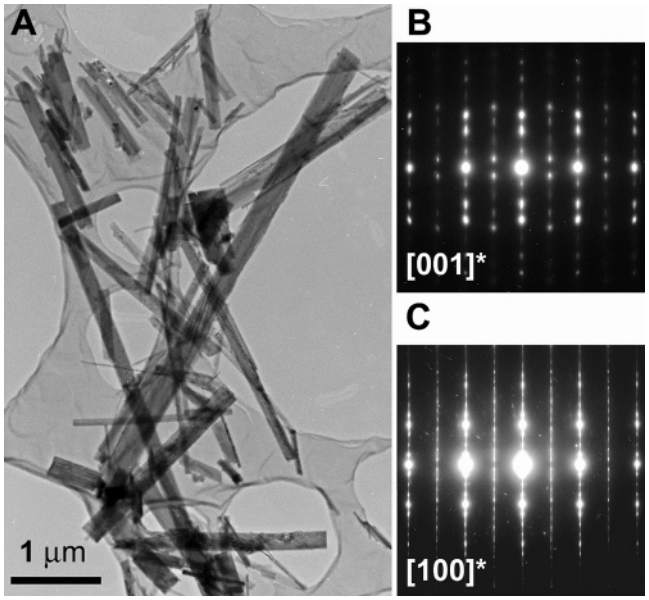

Figure 3. Low-magnification TEM image and corresponding ED patterns along the most prominent zone axes of $H_2Ti_3O_7$ nanorods of sample **NR-2**.

synthesized by the hydrothermal method depending on the starting materials.[20] This makes the interpretation of the XRD data even more ambiguous.

***NR-2-AIR** Sample.* XRD data (Figure 2D) for annealed in air sample **NR-2** evidence the formation of a metastable modification of titanium dioxide (TiO_2-B; monoclinic, $a = 1.218$ nm, $b = 0.374$ nm, $c = 0.653$ nm, $\beta = 107.05°$).[16] Similar results were previously obtained by several research groups.[15,21]

TEM. Transmission electron microscopy was applied to investigate the microstructure of the nanorods, and the observed results are in agreement with XRD data.

***NR-2** Sample.* Figure 3A shows a typical low-magnification TEM image of as-prepared nanorods of **NR-2**. The sample mostly consists of rodlike particles of different sizes, in good agreement with the SEM data. ED reveals a high crystallinity of the nanostructures, which was also confirmed by XRD. The ED patterns can be completely indexed in the monoclinic *C*2/*m* space group, using the $H_2Ti_3O_7$ unit cell parameters.[16] ED reveals two prominent growth directions: along [001] and along [100] (parts B and C of Figure 3, respectively). It should be noted that some unusual "broomlike" morphology has also been observed. A typical TEM image of such broomlike-type structure is shown in Figure 4. Selected area ED patterns of the multilayered end of the $H_2Ti_3O_7$ rod (a typical one is shown in the inset of Figure 4) clearly confirm the presence of the broomlike structure.

***NR-1-HYD** Sample.* TEM investigation reveals a high defect concentration in the synthesized nanorods. According to the ED data, this sample can be described either as highly defective hexa-titanate or as highly defective hepta-titanate.

***NR-2-AIR** Sample.* TEM shows the presence of two types of well crystallized nanostructures in the sample—rods and platelike structures (Figure 5). According to the ED data and the corresponding EDX data, they both are TiO_2-B, with a different morphology and growth direction, though. The rods are mainly oriented with their axis along [110], while the plates are mainly oriented along [001]. HREM investigation of TiO_2-B rods carries important information about the fine microstructure of nanorods. The existence of various types of defects, such as stacking faults, antiphase boundaries (APB), and twines, was

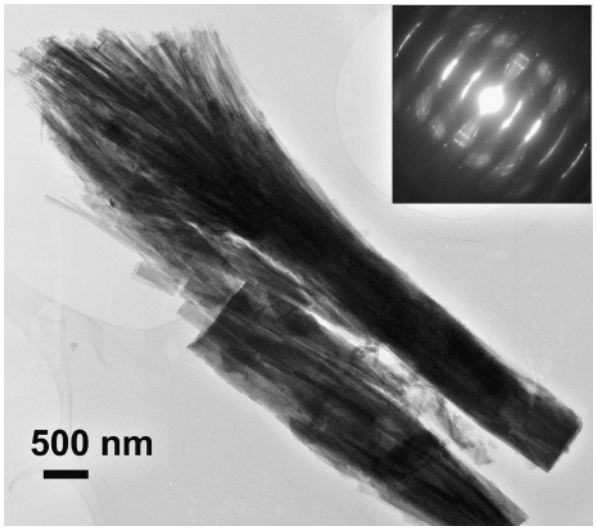

Figure 4. TEM image and corresponding electron diffraction pattern showing the existence of exfoliation at the end of thin rods of $H_2Ti_3O_7$ of sample **NR-2**.

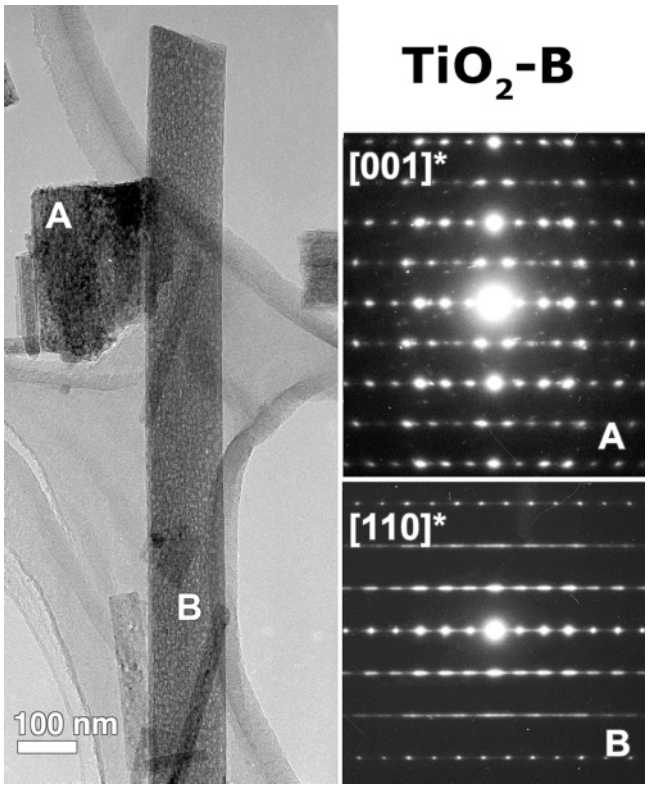

Figure 5. Low-magnification TEM image and corresponding ED patterns along the most prominent zone axes of TiO_2-B nanorods of sample **NR-2-AIR**.

revealed by HREM and ED. Figure 6A shows a typical [110] HREM image and its corresponding ED pattern of a strongly defective area of a lamellar TiO_2-B nanorod. The presence of streaks in the ED pattern (Figure 6B) is related to the presence of stacking faults perpendicular to the *c* axis. In the HREM image, one observes indeed the formation of numerous stacking faults and APB (Figure 6A). The ED pattern clearly demonstrates the presence of multiple twinning (Figure 6B). The reflections in the [00*l*] and [$\bar{3}$3*l*] rows are unsplit, whereas all reflections in the [$\bar{1}$1*l*] and [$\bar{2}$2*l*] rows are split, indicating the presence of mirror twins with a (001) twin plane. The [110] HREM image of a twinned region is shown in Figure 7. The

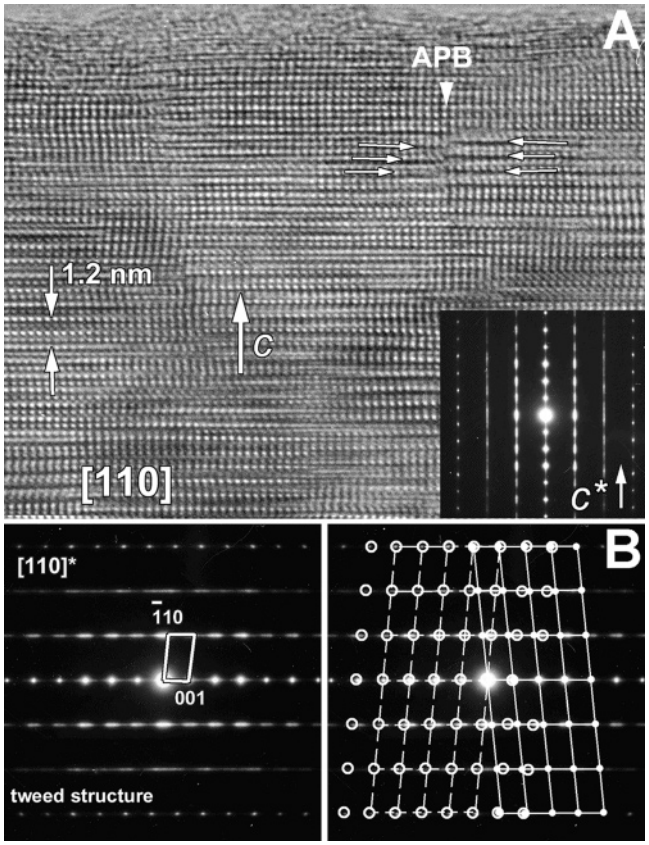

Figure 6. (A) [110] HREM image of a defective area of the lamellar TiO_2-B nanorod of sample **NR-2-AIR** showing the presence of the APB (marked by white arrows). (B) ED pattern taken from the tweed region and corresponding schematical representation.

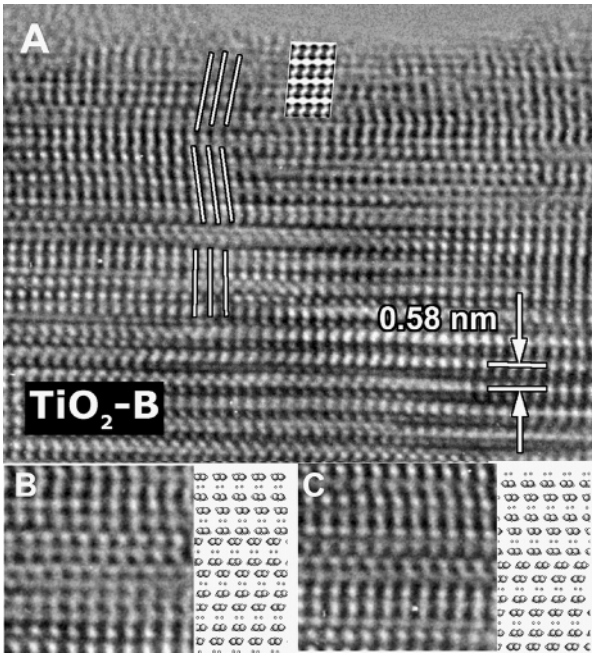

Figure 7. (A) [110] HREM image of nanorods of sample **NR-2-AIR** showing the twin region (inset: simulated images for $\Delta f = -40$ nm and $t = 40$ nm). (B and C) Enlargement of two different twins and corresponding model structure.

calculated image, using the structure parameters of TiO_2-B, is in good agreement with the experimental image where the black dots correspond to columns of Ti atoms. HREM images of two different twin arrangements are shown in Figure 7B and C. The formation of multiple twinning may be associated with a preconfiguration of the monoclinic structure of TiO_2-B in different variants.[22]

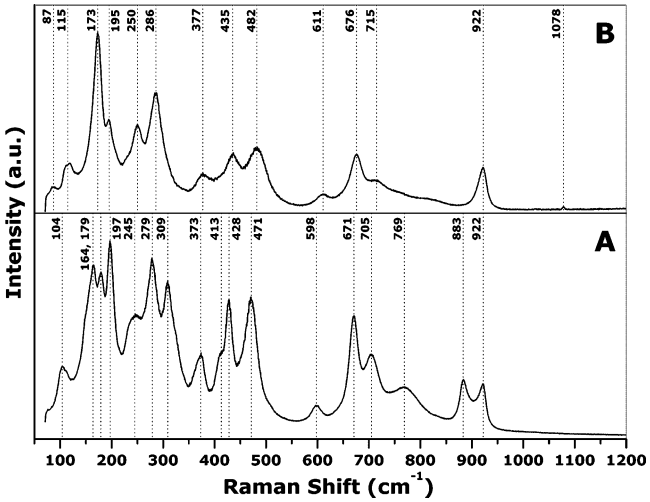

Figure 8. Raman spectra collected from the **NR-1** (A) and **NR-1-HYD** (B) samples.

Raman Spectroscopy. In the literature, the Raman spectra of various titanates and modification of titania are reported.[20,23,24]

NR-1 Sample. Figure 8A shows the Raman spectrum collected from the sample. XRD analysis reveals that this sample contains three $Na_2Ti_nO_{2n+1}$ phases ($n = 3, 4, 9$), but since the $Na_2Ti_3O_7$ phase is most abundant, the Raman spectrum is predominantly similar to spectra reported for sodium trititanate.[23,24] The set of observed bands and spectrum features agrees fairly well with the reported Raman data for $Na_2Ti_3O_7$; however, the relative intensities of the peaks differ.[24] This may be assigned to the textured microstructure of the sodium trititanate nanorods that are mostly continuous and roughly parallel to each other.

The bands at approximately 104, 197, 245, 279, 309, 373, 413, 428, and 471 cm^{-1} observed for the **NR-1** nanorods are quite similar to the reported data.[23] Additional expected bands representing the Na−O−Ti stretching vibration (∼279 and ∼309 cm^{-1}) are also observed in the low-wavenumber region.[25] However, inspection of the high-wavenumber region (500−1000 cm^{-1}) clearly shows the existence of bands shift toward the high-frequency region compared to the reported data.[23] These bands are mostly connected to Ti−O−Ti stretching vibrations and can be ascribed to the difference in Ti−O bond lengths in as-prepared $Na_2Ti_3O_7$ nanorods in comparison with sodium trititanate in the work of Papp et al.[23]

NR-2 Sample. A Raman spectrum of the sample is presented in Figure 9A. The spectrum is basically similar to that obtained by Papp and co-workers for $H_2Ti_3O_7$.[23] It should be noticed that we did not observe two bands reported by Papp.[23] They correspond to the Na−O−Ti stretching vibration (∼176 cm^{-1}) and the stretching vibration of short Ti−O bonds involving nonbridging oxygen coordinated with sodium ions (∼920 cm^{-1}). EDX microanalysis of **NR-2** confirmed the absence of sodium in the sample, whereas Papp et al. found 6% sodium in $H_2Ti_3O_7$ after the ion exchange process.[23] Given the fact that there are practically no Na^+ ions in the **NR-2** sample, we did not observe the bands mentioned above. In agreement with a previous study,[25] all bands detected for the $H_2Ti_3O_7$ nanorods represent a different titanium and oxygen stretching vibration in the TiO_6 octahedra.

NR-1-HYD Sample. A Raman spectrum is shown in Figure 8B. The spectrum is in excellent agreement with those reported

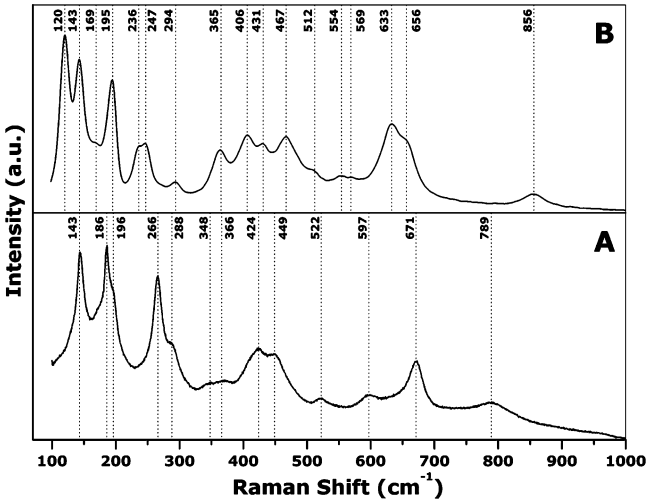

Figure 9. Raman spectra collected from the **NR-2** (A) and **NR-2-AIR** (B) samples.

for $Na_2Ti_6O_{13}$.[20] The weak band at ~1078 cm^{-1} in the Raman spectrum of the **NR-1-HYD** sample was observed in the high-frequency region. This band may be related to an admixture of sodium carbonate.[26]

***NR-2-AIR** Sample.* Figure 9B shows the Raman spectrum of the as-prepared TiO_2-B nanorods. The band positions for the TiO_2-B phase are in very good agreement with published data on either bulk or wirelike powders.[15a,16]

Discussion

All samples (**NR-1**, **NR-2**, **NR-1-HYD**, and **NR-2-AIR**) have a similar morphology, but their crystal structures are different and following structural transformations are schematically shown in Figure 10.

In the literature, the question of what are the products of hydrothermal reaction of NaOH with different titania precursors is intensively discussed;[12−15] in some articles, authors argue on the basis of EDX data mainly that direct formation of hydrogen tri-titanate ($H_2Ti_3O_7$) without an additional washing procedure is possible.[13] Sodium tri-titanate ($Na_2Ti_3O_7$) and hydrogen tri-titanate ($H_2Ti_3O_7$) are two closely related structures. The main building blocks are TiO_6 octahedra, which share edges to form a one-dimensional slab. These slabs form a two-dimensional layer by sharing the octahedral vertices (see Figure 10C). $Na_2Ti_3O_7$ is built up from the same two-dimensional framework of the TiO_6 octahedra, but the interlayer space is filled by sodium atoms (see Figure 10B).[27] It should be mentioned that sodium and hydrogen atoms occupy different crystallographic positions.

In our investigation, sample **NR-1** is a product of the hydrothermal reaction without additional washing, while sample **NR-2** is ultrasonically treated with HCl solution (Scheme 1). According to XRD, **NR-1** is a mixture of three sodium titanates ($Na_2Ti_nO_{2n+1}$, $n = 3, 4, 9$). The EDX analysis clearly indicates the presence of sodium in the sample and the Ti/Na ratio is ~1.8 that corresponds to the interval of ratios 1.5 ($Na_2Ti_3O_7$) and 4.5 ($Na_2Ti_9O_{19}$). Since the Ti/Na atomic ratio is close to 1.5, one may expect that the main component in the mixture of titanates is sodium tri-titanate ($Na_2Ti_3O_7$). Raman spectroscopy also confirms that $Na_2Ti_3O_7$ is the major phase in the **NR-1** sample. Ultrasonic dispersion of the **NR-1** sample in 0.1 M HCl leads to the formation of layered hydrogen titanate ($H_2Ti_3O_7$). The EDX analysis reveals the presence of only titanium and oxygen in sample **NR-2**; no sodium was found in the sample.

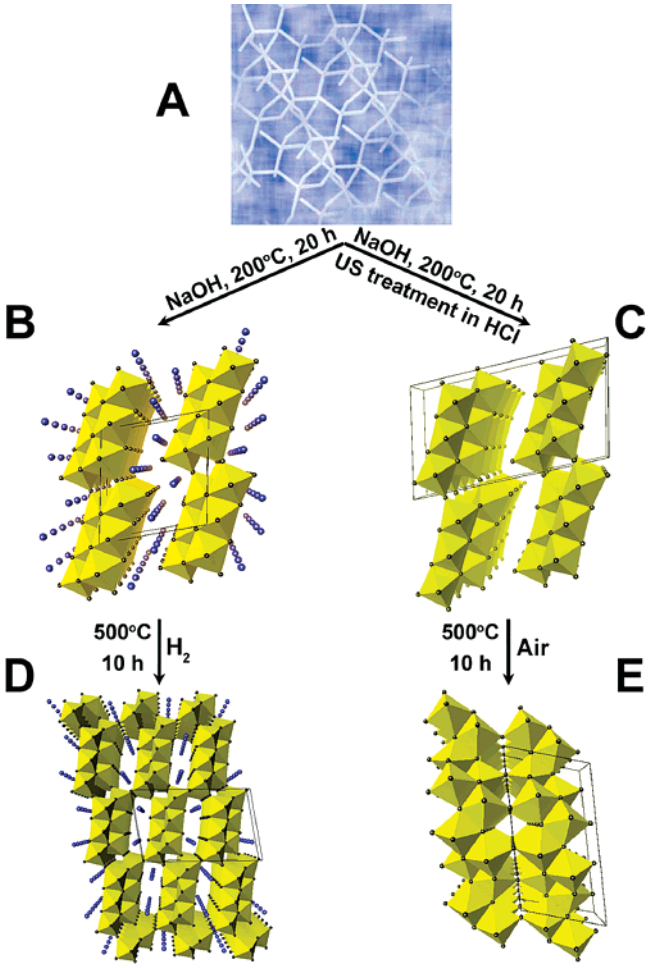

Figure 10. Schematic of the corresponding framework transformations: (A) amorphous $TiO_2 \cdot nH_2O$ gel (schematical figure); (B) $Na_2Ti_3O_7$; (C) $H_2Ti_3O_7$; (D) $Na_2Ti_6O_{13}$; (E) TiO_2-B.

Raman spectroscopy and TEM confirm that nanorods of sample **NR-2** have a $H_2Ti_3O_7$ crystal structure.

Our data clearly reveal that nanorods synthesized in one step by hydrothermal treatment in a NaOH solution contain sodium. Sodium-free nanorods of hydrogen titanate ($H_2Ti_3O_7$) can only be produced due to an ion exchange reaction with acid. A reaction of sodium titanate nanorods with hydrochloric acid maintains the particle morphology but modifies the crystal structure. Transformation of sodium titanate nanorods to hydrogen tri-titanate nanorods during the ion exchange reaction is accompanied by exfoliation of the zigzag ribbon layers in the thin rods. Indication for that is the formation of unusual particles with a broomlike morphology (Figure 4).

In the literature, well crystallized TiO_2 precursors (rutile,[21a] anatase,[11a,15,21b] and brookite[20]) are used for the preparation of nanorods of sodium titanates by hydrothermal treatment with NaOH. The temperature of the hydrothermal syntheses varies from 150 to 200 °C. Decreasing the temperature (130−150 °C) and using crystalline precursors leads to the formation of nanotubes of titania-related compounds.[13,15,28] In contrast, in the current investigation, amorphous titania gel was used as a starting material. Decreasing the temperature of the synthesis from 200 to 110 or 160 °C while keeping all other synthetic conditions constant does not lead to the formation of nanostructures. The samples are highly amorphous, and only a few extremely broad maxima corresponding to $H_2Ti_3O_7$ are present on XRD patterns. Apparently, the nature of the precursors plays an important role in the formation of the titanate nanostructures

and 20 h hydrothermal treatment at 160 °C or lower temperatures is not sufficient for crystallization of amorphous gel to ordered nanostructures.

According to published data,[15,21] the thermal treatment of nanorods of $H_2Ti_3O_7$ leads to the formation of nanorods of the TiO_2-B phase. The crystal structure of this polymorphous phase of titania consists of TiO_6 octahedra forming a three-dimensional framework with open channels (see Figure 10E). A sodium titanium dioxide bronze (Na_xTiO_2, $x \sim 0.2$) (air and moisture stable) with a structure containing practically the same three-dimensional framework of TiO_6 octahedra as TiO_2-B has been previously reported.[29] However, in the case of the bronze, the open channels are partially filled with sodium atoms. To investigate the possibility of producing nanorods of the Na_xTiO_2 bronze and TiO_2-B phase, we performed a thermal treatment at 500 °C of samples **NR-1** and **NR-2** in a hydrogen flow and air, respectively (Scheme 1).

SEM images indicate that the microstructure of the **NR-1-HYD** nanorods is quite similar to that of sample **NR-1** (parts B and A of Figure 1, respectively). However, in the XRD pattern, the peak positions and their relative intensities are not consistent with the diffraction pattern of Na_xTiO_2 bronze.[29] XRD shows that the sample is either hexa-titanate ($Na_2Ti_6O_{13}$) or hepta-titanate ($Na_2Ti_7O_{15}$). TEM reveals a highly defective structure of synthesized nanorods and does not provide an exact answer on the question of the crystal structure of sample **NR-1-HYD**. Moreover, the intergrowth of both structures can also not be excluded.[30]

Raman spectroscopy indicates that **NR-1-HYD** nanorods have a sodium hexa-titanate crystal structure. It can be seen not only from the comparison of the fingerprint spectra with literature data but also from the comparison of the crystal structures and Raman spectra (Figure 8) of the $Na_2Ti_3O_7$ and $Na_2Ti_6O_{13}$ compounds. The main difference in the oxygen frameworks of these structures (Figure 11) is that in $Na_2Ti_3O_7$ there are oxygen atoms (big black circles) belonging to one TiO_6 octahedron; consequently, the coordination number is one titanium atom at a distance of 1.71 Å and one sodium atom at a longer distance of 2.23 Å. Such a Ti−O distance is comparable with the apical Ti−O bond in the TiO_5 pyramids in Na_2TiSiO_5 (1.66 Å), and $Ba_2TiSi_2O_8$ (1.70 Å), where it is regarded as a "double" Ti−O bond.[25]

In the crystal structure of $Na_2Ti_6O_{13}$, all oxygen atoms belong to at least two octahedra (see Figure 11B). Transformation of the crystal structure of $Na_2Ti_3O_7$ to the structure of $Na_2Ti_6O_{13}$ can be described as a condensation of the two-dimensional layers of octahedra to a three-dimensional structure by sharing exactly these one-coordinated oxygen atoms (big black circles) (Figure 11). It means that there are no terminal oxygen atoms in the crystal structure of $Na_2Ti_6O_{13}$; all of them become linearly coordinated by two titanium atoms. The TiO_6 octahedra in $Na_2Ti_6O_{13}$ are more regular, there are no very long (2.2 Å) or very short (1.7 Å) Ti−O distances.

Comparison of the collected Raman spectra of samples **NR-1** and **NR-1-HYD** gives clear proof that the reaction shown in Scheme 2 takes place during annealing of sample **NR-1** in a hydrogen flow. The observed spectrum for sample **NR-1-HYD** is basically similar to that of the $Na_2Ti_3O_7$ nanorods (Figure 8). However, in the spectrum of sample **NR-1-HYD**, the bands at 309 and 883 cm^{-1} and splitting of the band at 173 cm^{-1} disappeared compared to the spectrum of sample **NR-1**. It seems quite reasonable, because these bands correspond to stretching Ti−O and Na−O vibrations including terminal oxygen atoms in the structure of $Na_2Ti_3O_7$. The band at 883 cm^{-1} corresponds

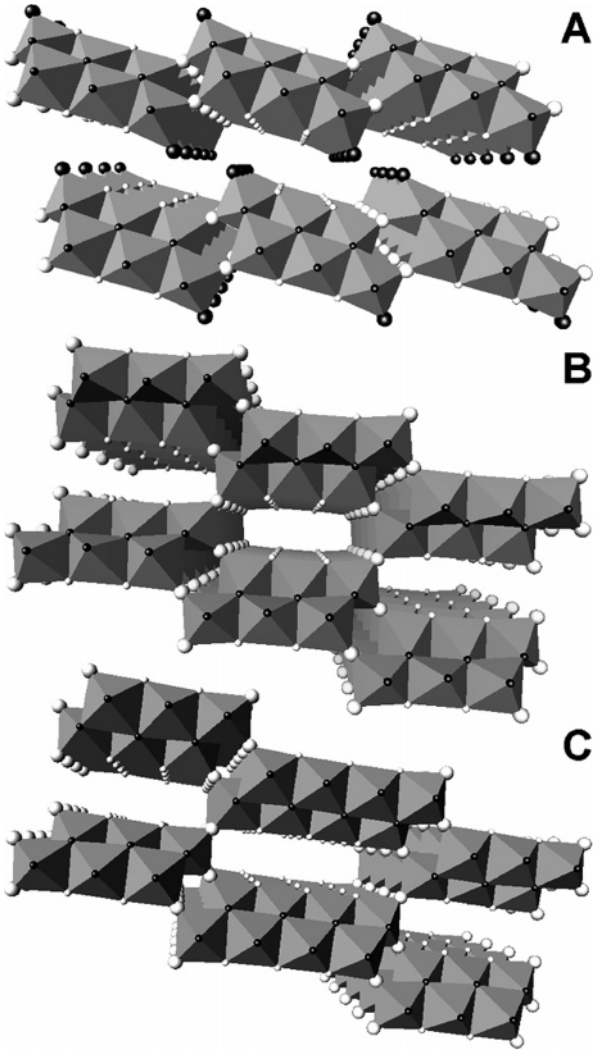

Figure 11. General view of the crystal structure of $Na_2Ti_3O_7$ (A), $Na_2Ti_6O_{13}$ (B), and $Na_2Ti_7O_{15}$ (C) phases. Sodium atoms were omitted for clarity. Different types of oxygen atoms are shown: (small black circles) oxygen atoms that belong to more than two TiO_6 octahedra, with high coordination numbers of 3 and 4; (small white circles) oxygen atoms that belong to two edge-sharing TiO_6 octahedra, with a coordination number of 2 and a Ti−O−Ti angle of ∼105°; (big white circles) oxygen atoms that belong to two corner-sharing octahedra, with a coordination number of 2 and a Ti−O−Ti angle of ∼180°; (big black circles) oxygen atoms that belong only to one TiO_6 octahedron, with a coordination number of one titanium atom at a distance of 1.71 Å and one sodium atom at a longer distance of 2.23 Å.

SCHEME 2

$$2\ Na_2Ti_3O_7 \xrightarrow[H_2]{500\,^\circ C,\ 10\ h} Na_2Ti_6O_{13} + Na_2O$$

to stretching vibration of the short Ti−O bond (1.71 Å),[32] while the bands at 173 and 309 cm^{-1} are believed to be due to the probable presence of a type of Na−O−Ti bond in $Na_2Ti_3O_7$ with a relatively short Na−O distance (2.23 Å).

It should be emphasized that the difference in the crystal structure of hexa- and hepta-titanate is only in the number of octahedra forming the slabs: in the case of $Na_2Ti_6O_{13}$, all slabs contain three octahedra, while, in the case of $Na_2Ti_7O_{15}$, three octahedra slabs alternate with four octahedra slabs (Figure 11B and C). In contrast with $Na_2Ti_6O_{13}$, there are short Ti−O bonds (1.70 Å) in the crystal structure of $Na_2Ti_7O_{15}$ that are similar to the ones in sodium tri-titanate.[19] The Raman spectrum of **NR-1-HYD** (Figure 8B) shows that the band corresponding to

such short Ti−O stretching vibrations is not present. The absence of this band is an additional argument for the abundant formation of $Na_2Ti_6O_{13}$ in the **NR-1-HYD** sample.

Also, Raman spectroscopy gives some additional hints that the reaction shown in Scheme 2 takes place. In the Raman spectrum of sample **NR-1-HYD**, the weak band at ~1078 cm^{-1} was observed in the high-frequency region which does not belong to any sodium titanates. This band may be related to an admixture of sodium carbonate in the **NR-1-HYD** sample.[26] The sample was stored in air after the thermal treatment in a hydrogen flow, and the presence of an admixture of Na_2CO_3 can be explained by taking into account the interaction between CO_2 from air with sodium oxide that is formed during the dimerization reaction.[31]

As neither XRD nor TEM allows distinguishment between hexa- and hepta-titanate in the **NR-1-HYD** sample, we can only suppose that nanorods of this sample have the $Na_2Ti_6O_{13}$ structure, as suggested by Raman spectroscopy data.

NR-2-AIR Sample. Annealing of sample **NR-2** in air leads to the expected formation of nanorods of TiO_2-B. The XRD pattern and Raman spectrum are in excellent agreement with those reported in the literature.[15a,16] SEM reveals that the microstructure of the sample after calcination is retained (Figure 1D); no morphology changes are observed. At the same time, a thermal treatment of $H_2Ti_3O_7$ leads to a considerable decrease of the average size and a narrowing of the size distribution of the nanorods (see Table 1).

TEM also confirms that nanorods in the **NR-2-AIR** sample have TiO_2-B crystal structure. Besides the formation of nanorods with their axis oriented along [110], TEM indicates also the formation of platelike particles oriented along [001]. Apparently, the calcination process and the removal of water from the $H_2Ti_3O_7$ leads to this particular destruction of the nanorods and the formation of platelike particles resulting in narrowing of the size distribution of the particles observed by SEM and TEM. The existence of various types of defects, such as stacking faults, antiphase boundaries (APB), and twines, was revealed by HREM and ED. It should be emphasized that the formation of antiphase boundaries and stacking faults has a strong influence on the electrochemical behavior of many transition metal oxides, for example, $LiCoO_2$ and $LiMnO_2$.[33] Therefore, in the case of lithium ion intercalation into nanorods of TiO_2-B[15] and hydrogen titanate,[28] structural defects may have a strong influence on the electrochemical properties and should not be neglected.

The formation of TiO_2-B from hydrogen titanate has been studied in detail by Feist et al.[16] They show that, upon heating, $H_2Ti_3O_7$ demonstrates a multistep weight loss behavior with the appearance of distinct structural intermediates. Upon complete dehydration, the TiO_2-B phase with a tunnel structure is formed. Our thermal analysis results of $H_2Ti_3O_7$ nanorods are in good agreement with those reported by Feist et al.[16] **NR-2** also exhibits two distinct mass loss steps: the first one is due to the release of physisorbed water molecules, while the other corresponds to the loss of lattice water molecules (moles of H_2O/moles of titanate ~ 1).

We have successfully prepared several types of titania based nanorods and studied their transformation, as schematically illustrated in Figure 10. First, the hydrothermal treatment of $TiO_2 \cdot nH_2O$ (Figure 10A) in NaOH results in the formation of $Na_2Ti_3O_7$ nanorods with small admixtures of $Na_2Ti_4O_9$ and $Na_2Ti_9O_{19}$ (Figure 10B). After acid treatment by ultrasonic dispersion of the nanorods of sodium tri-titanates in HCl, the ion exchange of protons for sodium ions leads to the formation of hydrogen titanate ($H_2Ti_3O_7$) nanorods (Figure 10C). Upon a thermal treatment of nanorods of the layered $Na_2Ti_3O_7$ and $H_2Ti_3O_7$ in an atmosphere of hydrogen and air, the formation of nanorods of sodium hexa-titanate ($Na_2Ti_6O_{13}$) (Figure 10D) and metastable TiO_2-B phases (Figure 10E) with a three-dimensional framework is observed.

The achievement of a uniform distribution and controlled growth of nanorods has great advantages with respect to the potential applications of such nanostructured materials. The mechanism of the nanorod crystallization under hydrothermal conditions is therefore under investigation.

Conclusions

Nanorods of various titanates and metastable TiO_2-B were successfully produced by a simple approach, based on the hydrothermal treatment of an amorphous $TiO_2 \cdot nH_2O$ gel in a concentrated NaOH solution. We have shown that as-prepared nanorods contain sodium and have the sodium tri-titanate crystal structure, while hydrogen tri-titanate nanorods can be easily produced by a treatment in acid solution. Both types of nanorods are mostly continuous and in the case of $Na_2Ti_3O_7$ arranged roughly parallel to one another. We also found that the nanorods of the metastable TiO_2-B phase can be prepared by a low-temperature calcination of the $H_2Ti_3O_7$ nanorods. Detailed Raman studies allowed us to propose the formation of $Na_2Ti_6O_{13}$ as the abundant phase upon thermal treatment of sodium tri-titanate nanorods in a hydrogen flow.

The HREM and ED investigation of the nanorods revealed the presence of numerous structural defects in the synthesized nanostructures. The large number of antiphase boundaries and stacking faults can be attributed to the exfoliation of the zigzag ribbon layers in the two-dimensional titanates as well as to the condensation of the layers of TiO_6 octahedra into a three-dimensional framework.

Acknowledgment. We are grateful to Dr. A. V. Olenev for the EDX analysis and N. V. Lyskov for the TGA measurements. This work is partially supported by RFBR (Grant No. 04-03-32295) and LSSP (Grant No. NSH-2033.2003.3). K.A.K. thanks the Max-Planck Society for a research fellowship, and Y.V.K. thanks the FY2005 JSPS Postdoctoral Fellowships for Foreign Researchers.

References and Notes

(1) (a) Patzke, G. R.; Krumeich, F.; Nesper, R. *Angew. Chem., Int. Ed.* **2002**, *41*, 2446. (b) Rao, C. N. R.; Deepak, F. L.; Gundiah, G.; Govindaraj, A. *Prog. Solid State Chem.* **2003**, *31*, 5. (c) Xia, Y.; Yang, P.; Sun, Y.; Wu, Y.; Mayers, B.; Gates, B.; Yin, Y.; Kim, F.; Yan, H. *Adv. Mater.* **2003**, *15*, 353. (d) Limmer, S. J.; Cao, G. *Adv. Mater.* **2003**, *15*, 427. (e) Li, D.; Xia, Y. *Adv. Mater.* **2004**, *16*, 1151.

(2) Limmer, S. J.; Cao, G. *Adv. Mater.* **2003**, *15*, 427.

(3) Yi, D. K.; Yoo, S. J.; Kim, D.-Y. *Nano Lett.* **2002**, *2*, 1101.

(4) (a) Miao, Z.; Xu, D.; Ouyang, J.; Guo, G.; Zhao, X.; Tang, Y. *Nano Lett.* **2002**, *2*, 717. (b) Lei, Y.; Zhang, L. D. *J. Mater. Res.* **2001**, *16*, 1138. (c) Zhang, M.; Bando, Y.; Wada, K. *J. Mater. Sci. Lett.* **2001**, *20*, 167. (d) Miao, L.; Tanemura, S.; Toh, S.; Kaneko, K.; Tanemura, M. *J. Cryst. Growth* **2004**, *264*, 246.

(5) (a) Wu, J.-J.; Yu, C.-C. *J. Phys. Chem. B* **2004**, *108*, 3377. (b) Pradhan, S. K.; Reucroft, P. J.; Yang, F.; Dozier, A. *J. Cryst. Growth* **2003**, *256*, 83.

(6) Lei, Y.; Zhang, L. D.; Fan, J. C. *Chem. Phys. Lett.* **2001**, *338*, 231.

(7) Zhu, Y.; Li, H.; Koltypin, Y.; Hacohen, Y. R.; Gedanken, A. *Chem. Commun.* **2001**, 2616.

(8) Wang, G.; Li, G. *Eur. Phys. J. D* **2003**, *24*, 355.

(9) Xu, C.; Zhan, Y.; Hong, K.; Wang, G. *Solid State Commun.* **2003**, *126*, 545.

(10) Byrappa, K.; Yoshimura, M. *Handbook of Hydrothermal Technology*; William Andrew Publishing: New York, 2001; Chapter 1.

(11) (a) Zhang, Y. X.; Li, G. H.; Jin, Y. X.; Zhang, Y.; Zhang, J.; Zhang, L. D. *Chem. Phys. Lett.* **2002**, *365*, 300. (b) Yuan, Z. Y.; Colomer, J. F.;

Su, B. L. *Chem. Phys. Lett.* **2002**, *363*, 362. (c) Du, G. H.; Chen, Q.; Han, P. D.; Yu, Y.; Peng, L.-M. *Phys. Rev. B* **2003**, *67*, (035323) 1.

(12) (a) Kasuga, T.; Hiramatsu, M.; Hoson, A.; Sekino, T.; Niihara, K. *Adv. Mater.* **1999**, *15*, 1307. (b) Kasuga, T.; Hiramatsu, M.; Hoson, A. *Langmuir* **1998**, *14*, 3160.

(13) (a) Chen, Q.; Zhou, W.; Du, G. H.; Peng, L.-M. *Adv. Mater.* **2002**, *14*, 1208. (b) Du, G. H.; Chen, Q.; Che, R. C.; Yuan, Z. Y.; Peng, L.-M. *Appl. Phys. Lett.* **2001**, *79*, 3702. (c) Zhang, S.; Peng, L.-M.; Chen, Q.; Du, G. H.; Dawson, G.; Zhou, W. *Phys. Rev. Lett.* **2003**, *91*, 256103-1. (d) Zhang, S.; Chen, Q.; Peng, L.-M. *Phys. Rev. B* **2005**, *71*, 014104.

(14) Sun, X.; Li, Y. *Chem.—Eur. J.* **2003**, *9*, 2229.

(15) (a) Armstrong, A. R.; Armstrong, G.; Canales, J.; Bruce, P. G. *Angew. Chem., Int. Ed.* **2004**, *43*, 2286. (b) Armstrong, A. R.; Armstrong, G.; Canales, J.; Garsia, R.; Bruce, P. G. *Adv. Mater.* **2005**, *17*, 862. (c) Armstrong, G.; Armstrong, A. R.; Canales, J.; Bruce, P. G. *Chem. Commun.* **2005**, 2454.

(16) Feist, T. P.; Davies, P. K. *J. Solid State Chem.* **1992**, *101*, 275.

(17) Akimoto, J.; Takei, H. *J. Solid State Chem.* **1991**, *90*, 92.

(18) Andersson, S.; Wadsley, A. D. *Acta Crystallogr.* **1962**, *15*, 194.

(19) Wadsley, A. D.; Mumme, W. G. *Acta Crystallogr., Sect. B* **1968**, *24*, 392.

(20) Meng, X.; Wang, D.; Liu, J.; Zhang, S. *Mater. Res. Bull.* **2004**, *39*, 2163.

(21) (a) Pavasupree, S.; Suzuki, Y.; Yoshikawa, S.; Kawahata, R. *J. Solid State Chem.* **2005**, *178*, 3110. (b) Yoshida, R.; Suzuki, Y.; Yoshikawa, S. *J. Solid State Chem.* **2005**, *178*, 2179.

(22) Van Tendeloo, G.; Lebedev, O. I.; Hervieu, M.; Raveau, B. *Rep. Prog. Phys.* **2004**, *67*, 1315.

(23) Papp, S.; Korosi, L.; Meynen, V.; Cool, P.; Vansant, E. F.; Dekany, I. *J. Solid State Chem.* **2005**, *178*, 1614.

(24) Bamberger, C. E.; Begun, G. M. *J. Am. Ceram. Soc.* **1987**, *70*, C-48.

(25) Su, Y.; Balmer, M. L.; Bunker, B. C. *J. Phys. Chem. B* **2000**, *104*, 8160.

(26) Jackson, K. D. O. *Internet J. Vib. Spectrosc.* [Online] **1998**, *2*, 3rd ed. (www.ijvs.com).

(27) Andersson, S.; Wadsley, A. *Acta Crystallogr.* **1961**, *14*, 1245.

(28) Lan, Y.; Gao, X. P.; Zhu, H. Y.; Zheng, Z. F.; Yan, T. Y.; Wu, F.; Ringer, S. P.; Song, D. Y. *Adv. Funct. Mater.* **2005**, *15*, 1310.

(29) Andersson, S.; Wadsley, A. *Acta Crystallogr.* **1962**, *15*, 201.

(30) Xu, F. F.; Bando, Y.; Kurashima, K.; Ogawa, H.; Inada, K. *J. Solid State Chem.* **2001**, *162*, 128.

(31) Geselbracht, M. J.; Noailles, L. D.; Ngo, L. T.; Pikul, J. H.; Walton, R. I.; Cowell, E. S.; Millange, F.; O'Hare, D. *Chem. Mater.* **2004**, *16*, 1153.

(32) Ocana, M.; Garcia-Ramos, J. V.; Serna, C. J. *J. Am. Ceram. Soc.* **1992**, *75*, 2010.

(33) (a) Chabre, Y.; Parmetier, J. *Prog. Solid State Chem.* **1995**, *23*, l. (b) Wang, H.; Jang, Y.-I.; Chiang, Y.-M. *Electrochem. Solid-State Lett.* **1999**, *2*, 490. (c) Chiang, Y.-M.; Wang, H.; Jang, Y.-I. *Chem. Mater.* **2001**, *13*, 53. (d) Tessier, C.; Audry, C.; Bernard, P. *J. Electrochem. Soc.* **2005**, *152*, A1248.